

## Supporting Information

### **Job-Sharing Cathode Design for Li-O<sub>2</sub> Batteries with High Energy Efficiency Enabled by In-Situ Ionic Liquid Bonding to Cover Carbon Surface Defects**

Peili Lou,<sup>a,b</sup> Chilin Li,<sup>a,\*</sup> Zhonghui Cui<sup>a</sup> and Xiangxin Guo<sup>a,\*</sup>

<sup>a</sup>State Key Laboratory of High Performance Ceramics and Superfine Microstructure, Shanghai Institute of Ceramics, Chinese Academy of Sciences, Shanghai 200050, China

<sup>b</sup>University of Chinese Academy of Sciences, Beijing, 100039, China

\*E-mail: [chilinli@mail.sic.ac.cn](mailto:chilinli@mail.sic.ac.cn) or [xxguo@mail.sic.ac.cn](mailto:xxguo@mail.sic.ac.cn)

## Methods

**Sample preparation.** Ru-IL-MWCNT composites were prepared according to Ref.[27]. In a typical synthesis, 30 mg multi-wall carbon nanotubes (MWCNTs, Shenzhen Nanotech. Port. Co., Ltd) were added into 60 mL ethylene glycol (EG, Sinopharm chemical reagent Co., Ltd) with the suspension being stirred for 30 min, and then 1.1 mL IL 1-butyl-3-methyl imidazolium tetrafluoroborate (BmimBF<sub>4</sub>, Sigma Aldrich) was added into this CNT-EG suspension. The CNT-IL-EG solution was sonicated for 5 min and stirred for 4 h. Here IL BmimBF<sub>4</sub> was used to disentangle and disperse CNT clusters and finally to cap individual CNT through a cation- $\pi$  interaction.[24-26,30] After that, 22.5 mg RuCl<sub>3</sub> (Sigma Aldrich) and 1.5 mL 0.10 M HCl (Sinopharm chemical reagent Co., Ltd) were further added into this solution, which was sonicated for another 5 min. The mixture was refluxed at 198 °C in oil bath for 3 h. Fine Ru nanoparticles were finally precipitated on IL-capped CNTs with their surfaces also being decorated by IL through an electrostatic interaction between RuCl<sub>4</sub><sup>-</sup> and Bmim<sup>+</sup>. [27] The resulting products were washed with deionized water and acetone for several times and collected by centrifugation. To confirm the functions of Ru and IL in Ru-IL-MWCNT, we also prepared some control samples, including (1) IL-MWCNT composites free of Ru nanoparticles, (2) Ru-MWCNT composites free of IL coating layer, as well as (3) Ru-MWCNT-IL composites where IL was added after Ru nucleation. For IL-MWCNT, 30 mg MWCNTs and 1.1 mL BmimBF<sub>4</sub> were dispersed 60 mL EG. The CNT-IL-EG solution was sonicated for 5 min and stirred for 4 h. For

Ru-MWCNT, 30 mg MWCNTs were added into 60 mL EG with the suspension being stirred for 30 min. Then, 22.5 mg  $\text{RuCl}_3$  and 1.5 mL 0.10 M HCl were added into this solution, which was sonicated for 5 min. The mixture was refluxed at 198 °C in oil bath for 3 h. For Ru-MWCNT-IL, the early steps are similar to these for Ru-MWCNT, which are followed by an extra step where 1.1 mL  $\text{BmimBF}_4$  was added into EG after Ru nucleation with further stirring for 4 h. These final solid products were dried at 90 °C in a vacuum oven for overnight.

**Material characterization.** The morphology and microstructure of pristine and cycled electrodes were observed through a transmission electron microscope (TEM, JEOL JEM-2100F TEM) and a FEI Magellan 400 extreme high resolution scanning electron microscope (SEM), where dark-field and bright-field scanning TEM (STEM) and energy-dispersive X-ray spectroscopy (EDS) elemental mappings were collected. X-ray diffraction (XRD) measurements of the pristine and discharged samples were carried out at the BL14B1 Beamline of the Shanghai Synchrotron Radiation Facility. The surface and subsurface compositions of pristine and cycled samples (as well as commercial reference samples) were analyzed by X-ray photoelectron spectroscopy (XPS, ESCALAB-250) with an Al anode source. Raman spectra at corresponding reaction stages were recorded in Thermo DXR with an excitation wavelength of 532 nm. Nitrogen adsorption-desorption isotherms at 77 K were measured on a Micromeritics Tristar 3000 system.

The oxygen cathodes were prepared by mixing Ru-IL-MWCNT (or IL-MWCNT, Ru-MWCNT) with polyvinyl difluoride (PVDF) binder in a weight ratio of 9:1, and then pressed onto a stainless steel (Alfa Aesar, 200 mesh screen) with a thickness of 100  $\mu\text{m}$  followed by drying in vacuum at 60 °C for at least 12 h. The mass loading of Ru-IL-MWCNT was about 8  $\text{mg cm}^{-2}$ . Two-electrode Swagelok-type Li-O<sub>2</sub> cells were assembled in an Ar-filled glove box (M-Braun, Germany) with both moisture and oxygen contents below 0.1ppm. Components for each battery include a 0.25-mm-thick lithium anode, a glass fiber ( $\Phi$ 12mm, GF/B, Whatman) separator saturated with dimethyl sulfoxide (DMSO) electrolyte dissolving 0.5M  $\text{LiClO}_4$  inside ( $\text{H}_2\text{O} < 5$  ppm), and an aforementioned oxygen cathode. After assembly, each Li-O<sub>2</sub> battery was sealed in a home-made airtight stainless steel chamber (190 mL) with both inlet and outlet tubes for oxygen flowing. Under static oxygen atmosphere ( $\sim 10^5$  Pa), these cells were firstly rested for 4 h, and then measured in a galvanostatic mode at room temperature with different current densities from 25  $\text{mA g}^{-1}$  to 300  $\text{mA g}^{-1}$  in both the protocols of voltage and capacity cut-off by using an Arbin BT2000 battery test

system. The discharge-charge capacities were calculated based on the weight of active materials. Galvanostatic intermittent titration technique (GITT) was performed at a fixed current density of  $50 \text{ mA g}^{-1}$  with a relaxation time of 6 h between 2.5 V and 4.3 V. In order to check whether the voltage can easily relax to the equilibrium value ( $U_{eq}$ ) even after a long-term cycling (at that time already with a slight increase of ohmic impedance), the cell is in advance cycled for 100 cycles at  $75 \text{ mA g}^{-1}$  before GITT measurement.

The cathodes of different discharged or charged stages were taken out from the cycled cells in Ar-filled glove box, and were washed with  $\text{CH}_3\text{CN}$  (purified with fresh activated molecular sieve,  $\text{H}_2\text{O} < 4 \text{ ppm}$ ) and then dried under vacuum. They were used for various characterizations such as XRD, SEM, TEM, XPS and Raman spectra. Note that all these samples were treated carefully without exposing to ambient air.

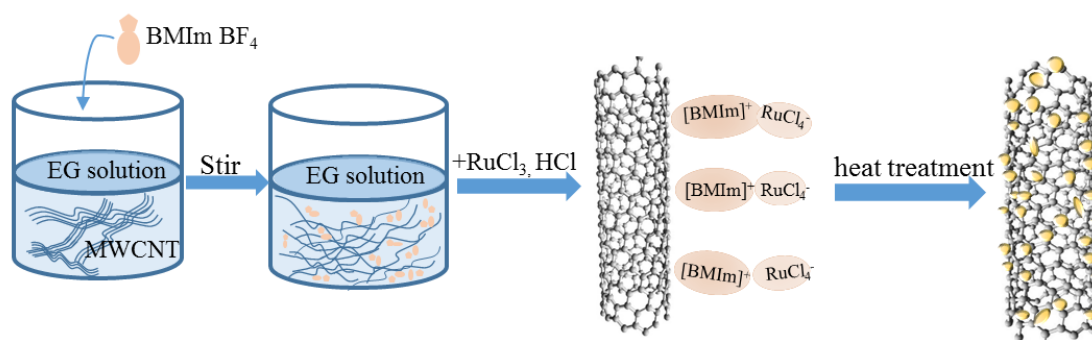


**Figure S1.** Schematic illustration of synthesis steps to Ru-IL-MWCNT composite. MWCNTs and BmimBF<sub>4</sub> were sequentially added into EG to form CNT-IL-EG solution. Here IL BmimBF<sub>4</sub> was used to disentangle and disperse CNT clusters and finally to cap individual CNT through a cation- $\pi$  interaction. Then RuCl<sub>3</sub> and HCl were further added into this solution, leading to a precipitation of fine Ru nanoparticles on IL-capped CNTs with nano-Ru surfaces also being decorated by IL through an electrostatic interaction between RuCl<sub>4</sub><sup>-</sup> and Bmim<sup>+</sup>.

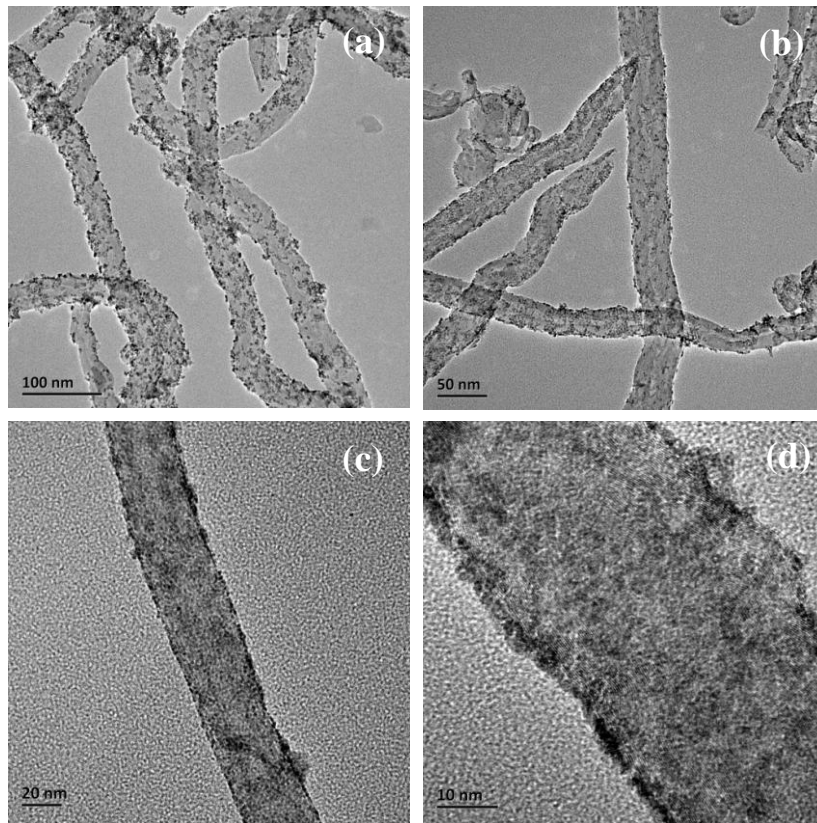


**Figure S2.** TEM images of Ru-IL-MWCNT with various magnification at different regions. Numerous fine Ru nanodots (2~3 nm) are uniformly dispersed on CNT surface without serious aggregating.

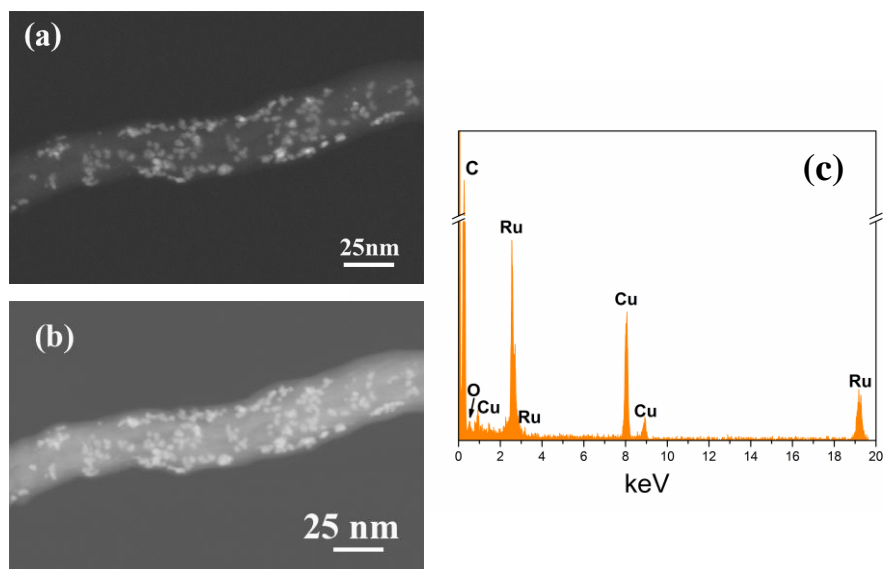


**Figure S3.** (a) High-angle annular-dark field (HAADF) image and (b) dark field STEM image of Ru-IL-MWCNT composite. (c) EDS of the corresponding region. Uniform loading of nano-Ru on CNT framework is clearly observed.

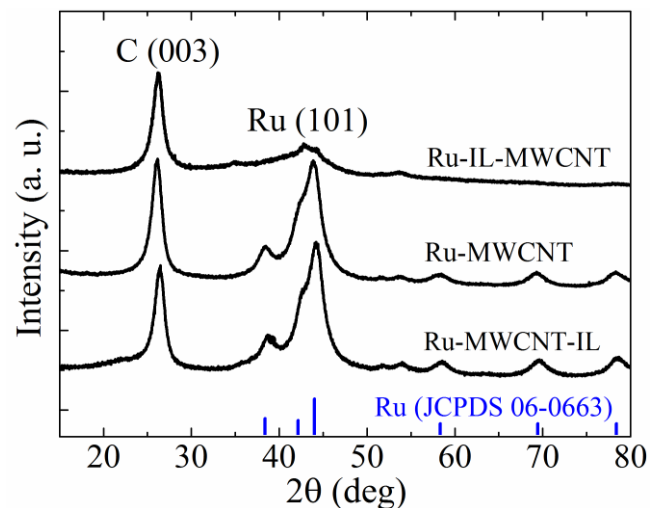


**Figure S4.** XRD patterns of Ru-IL-MWCNT, Ru-MWCNT and Ru-MWCNT-IL composites. For the former (Ru-IL-MWCNT), the broad diffraction peaks indicates a nanocrystalline structure of Ru. For another two control samples (Ru-MWCNT and Ru-MWCNT-IL), the diffraction peaks of Ru become much more intensified owing to crystallinity improvement and grain growth.

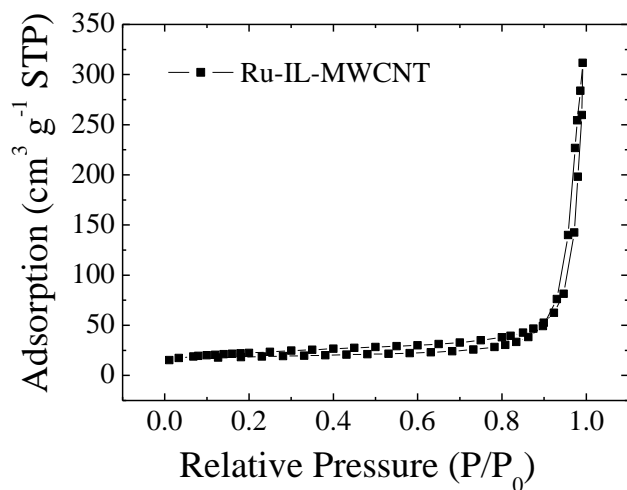


**Figure S5.** Nitrogen adsorption and desorption isotherms of Ru-IL-MWCNT composite. It displays a macroporosity-like feature with a surface area of  $79 \text{ m}^2 \text{ g}^{-1}$  from this BET measurement.

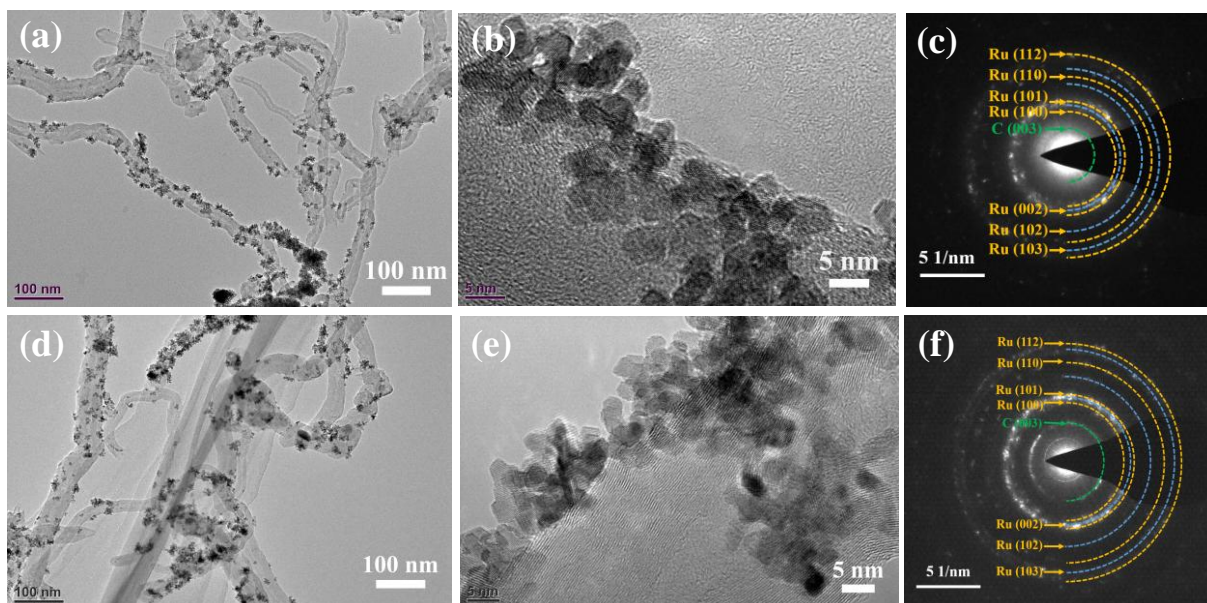


**Figure S6.** TEM images of (a,b) Ru-MWCNT and (d,e) Ru-MWCNT-IL with various magnification. SAED patterns of (c) Ru-MWCNT and (f) Ru-MWCNT-IL. For both samples, Ru nanoparticles (4~5 nm) are dispersed on CNT surface but with aggregating to a certain extent. The corresponding SAED patterns indicate crystallinity improvement of Ru with evident polycrystalline diffraction dots.

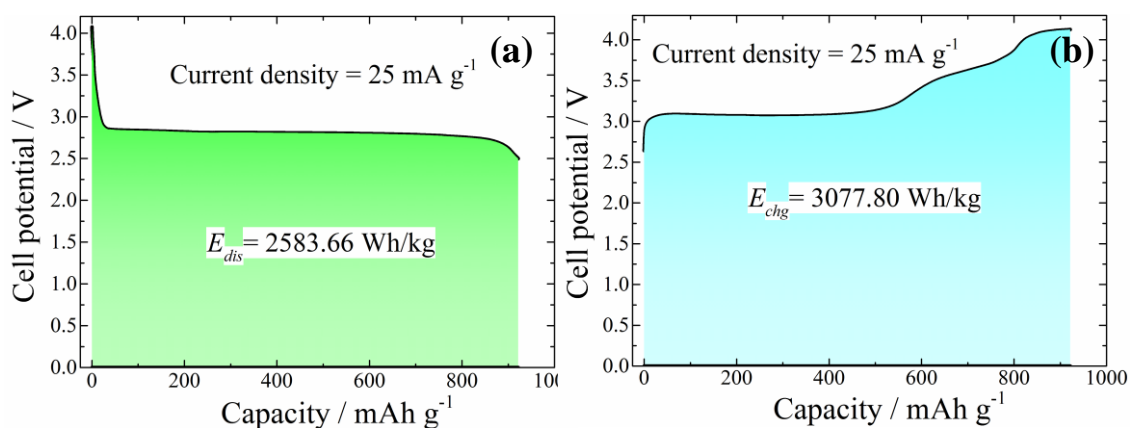


**Figure S7.** Typical (a) discharge and (b) charge curves at  $25 \text{ mA g}^{-1}$  for calculating the specific energy in the whole electrochemical region, where  $E_{dis}$  and  $E_{chg}$  are the energy densities of full discharge and charge processes respectively. It is used to estimate the round-trip energy efficiency ( $\text{RTE} = E_{chg} / E_{dis}$ ).

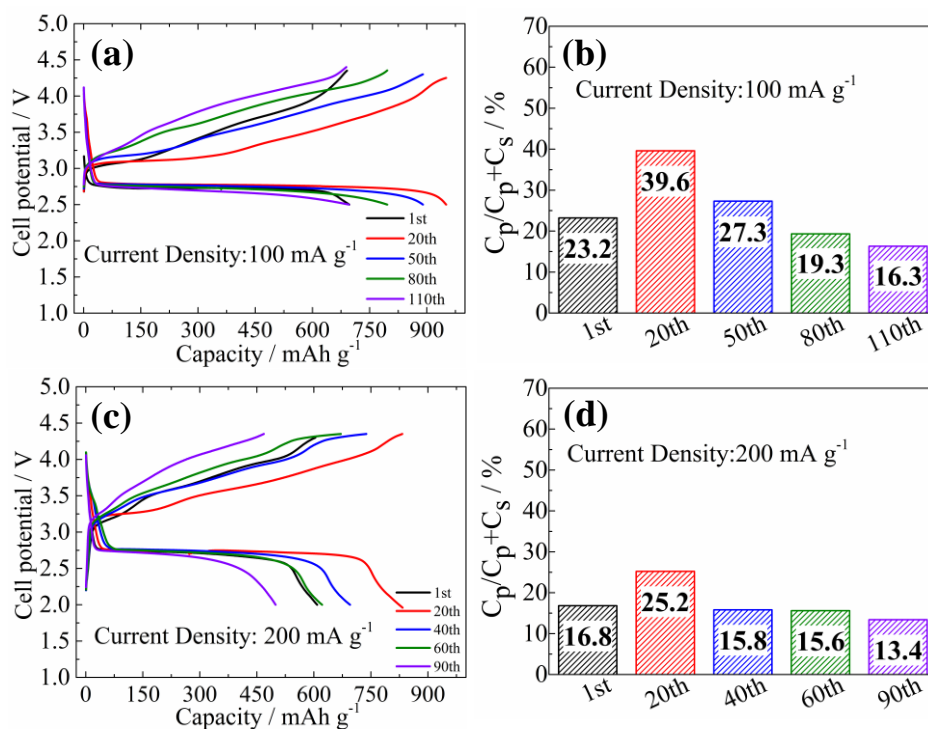


**Figure S8.** Typical galvanostatic charge-discharge curves of Ru-IL-MWCNT at higher current densities of (a) 100 mA g<sup>-1</sup> and (c) 200 mA g<sup>-1</sup> under a mode of voltage cut-off. The corresponding C<sub>p</sub>/(C<sub>p</sub>+C<sub>s</sub>) values depending on cycling number at (b) 100 mA g<sup>-1</sup> and (d) 200 mA g<sup>-1</sup>, where C<sub>p</sub> and C<sub>s</sub> denoting the charge capacities of plateau and sloped curve regions respectively. Note that for both the current densities the C<sub>p</sub>/(C<sub>p</sub>+C<sub>s</sub>) values increase abnormally during the early cycles (e.g. from 23% for the 1<sup>st</sup> cycle to 40% for the 20<sup>th</sup> cycle at 100 mA g<sup>-1</sup>) and then gradually decrease during the late long-term cycling (e.g. to 16 % after the 110<sup>th</sup> cycle). This is in accordance with the capacity activation during the early cycling followed by gradual capacity degradation during the late cycling.

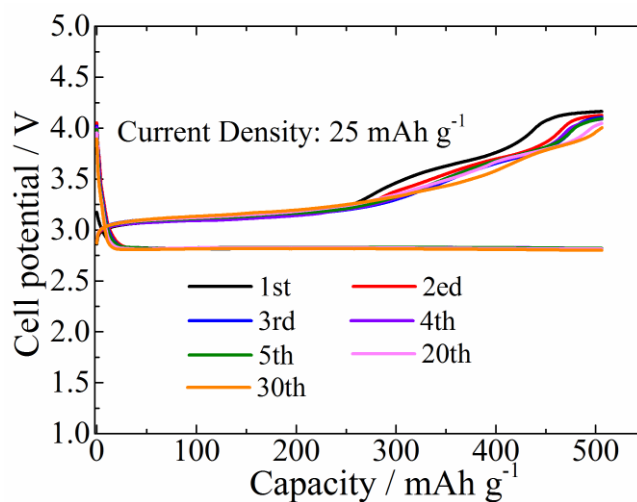


**Figure S9.** Typical galvanostatic charge-discharge curves of Ru-IL-MWCNT at  $25 \text{ mA g}^{-1}$  under a mode of capacity cut-off to  $500 \text{ mAh g}^{-1}$ . The OER capacity of sloped curve at the higher voltage (beyond near- $E_o$  plateau) is still observable even though under this small current density of  $25 \text{ mA g}^{-1}$ .

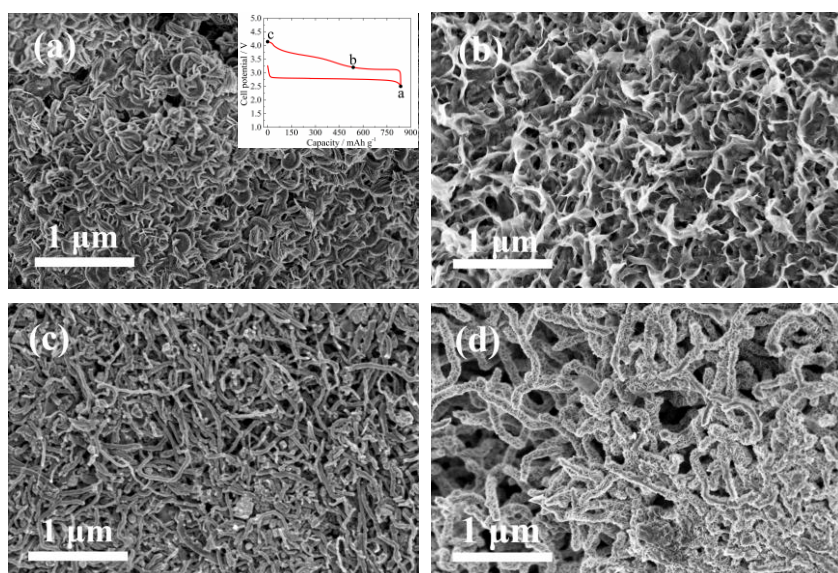


**Figure S10.** Overview SEM images of cycled Ru-IL-MWCNT electrodes at different stages under a current density of  $75 \text{ mA g}^{-1}$ : (a) Discharged to  $2.5 \text{ V}$  in the  $5^{\text{th}}$  cycle, (b) recharged to  $3.2 \text{ V}$  in the  $5^{\text{th}}$  cycle, (c) recharged to  $4.35 \text{ V}$  in the  $5^{\text{th}}$  cycle, and (d) discharged to  $2.5 \text{ V}$  in the  $40^{\text{th}}$  cycle. Inset of (a): A typical cycling process for Ru-IL-MWCNT with labelling at the corresponding discharge/charge stages. The products deposit on CNT surface in a manner of stacking of nanosheet bundles after deep discharge, whereas the nanosheet-like products become thinner and sparse with the progress of recharging until completely disappear when recharging above  $4 \text{ V}$ . The size of products also significantly depends on cycling number as shown in (d) with a well-defined stacking of nanosheet-like species almost everywhere on CNT surface after 40 cycles. The width of deposit (tens of nanometer) appears to be roughly one order of magnitude smaller than that (hundreds of nanometer) in the early discharged sample.

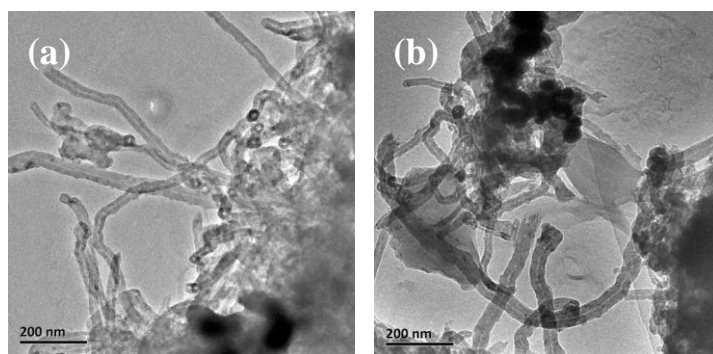


**Figure S11.** TEM images of Ru-IL-MWCNT electrode discharged to 2.5 V after 5 cycles at different regions. We can find that some of the CNT surfaces are still left uncovered in view of space squeeze of large-sized products.

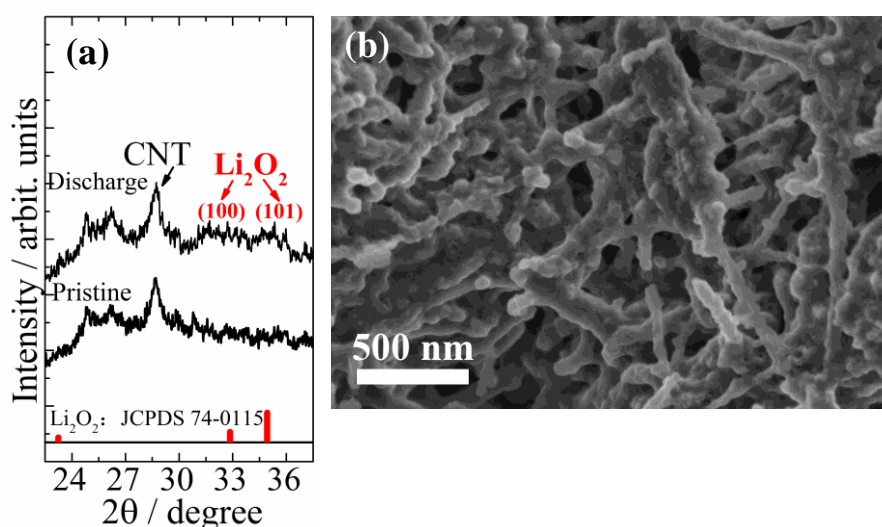


**Figure S12.** (a) XRD patterns of Ru-MWCNT discharged to 2.5 V and the pristine electrode. (b) SEM image of Ru-MWCNT electrode discharged to 2.5 V. Highly disordered structure of  $\text{Li}_2\text{O}_2$  product is observed after deep discharge as in the case of Ru-IL-MWCNT. However, the discharged Ru-MWCNT sample mainly displays colloidal coating on CNT instead of well-defined nanosheet stacking as observed in the discharged Ru-IL-MWCNT sample. The accelerated formation of colloidal carbonates due to a lack of IL layer discounts the benefit from the microstructure modification of  $\text{Li}_2\text{O}_2$  by Ru nanoparticles.

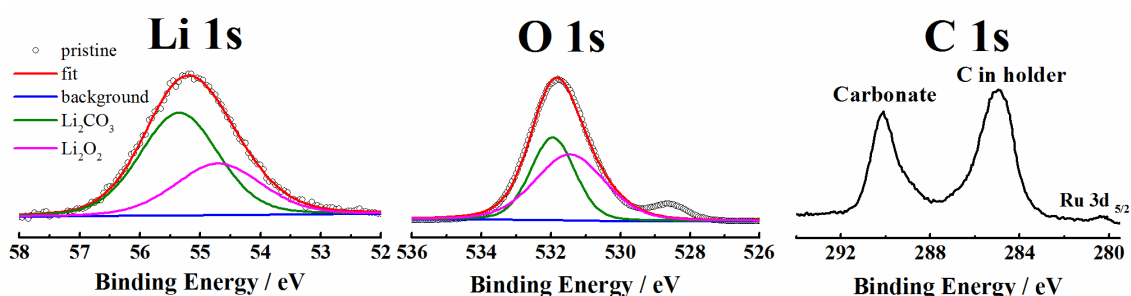


**Figure S13.** Surface sensitive XPS spectra of Li 1s, O 1s, C 1s and Ru 3d<sub>5/2</sub> of the Ru-MWCNT electrode after discharge to 2.5 V. A higher fraction of carbonate byproducts is detected compared with the case of Ru-IL-MWCNT at the corresponding discharge stage, indicating that the absence of IL protection accelerates the formation of carbonates.

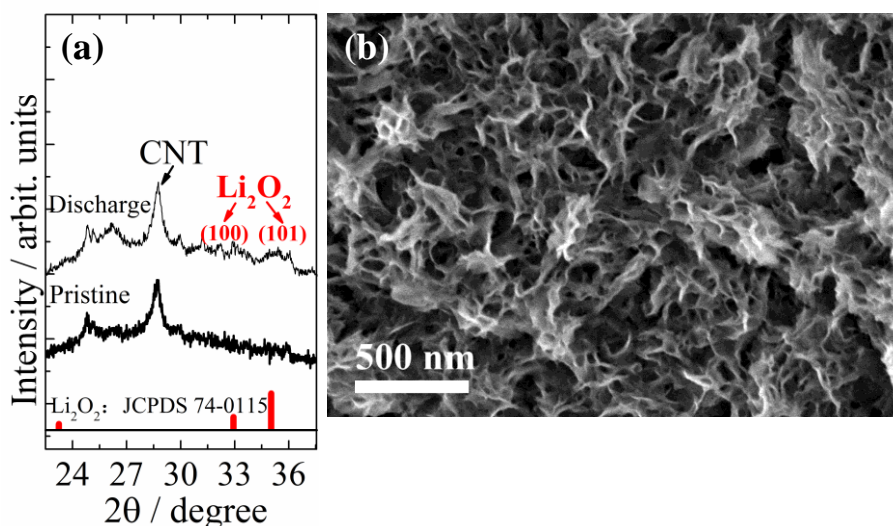


**Figure S14.** (a) XRD patterns of Ru-MWCNT-IL discharged to 2.5 V and the pristine electrode. (b) SEM image of Ru-MWCNT-IL electrode discharged to 2.5 V. Highly disordered structure of Li<sub>2</sub>O<sub>2</sub> product is observed after deep discharge as in the case of Ru-IL-MWCNT. The discharged Ru-MWCNT-IL sample shows the similar nanosheet stacking as the discharged Ru-IL-MWCNT sample. Even though the late addition of IL after Ru nucleation, the IL-coating existence still suppresses the formation of colloidal carbonates as observed in the Ru-MWCNT sample.